

## Detection of AGNs and quasars having significant proper motions according to Gaia data within SRG/eRosita X-Ray sources catalog

I. M. Khamitov<sup>1,2,3\*</sup>, I. F. Bikmaev<sup>1,3</sup>, M. R. Gilfanov<sup>4,5</sup>, R. A. Sunyaev<sup>4,5</sup>,  
P. S. Medvedev<sup>4</sup>, M. A. Gorbachev<sup>1,3</sup>, E. N. Irtuganov<sup>1,3</sup>

<sup>1</sup>*Kazan Federal University, Kazan, Russia*

<sup>2</sup>*TÜBİTAK National Observatory, Antalya, Turkey*

<sup>3</sup>*Tatarstan Academy of Sciences, Kazan, Russia*

<sup>4</sup>*Space Research Institute of Russian Academy of Sciences, Moscow, Russia*

<sup>5</sup>*Max-Planck Institute for Astrophysics, Garching, Germany*

Received October 31, 2022

### Abstract —

Based on a comparison of the SRG/eROSITA catalog of X-ray active stars and the Gaia catalog, a sample of 502 peculiar objects was obtained for which Gaia, on one hand, detects statistically significant values of parallax or proper motion and, on the other hand, registers signs of the non zero source extent in the optical band. In the  $\log(F_X/F_{\text{opt}}) - (G-RP)$  color diagram these objects are separated from the bulk of X-ray active stars and are located in the region typical for the galaxies with active nuclei. According to the SIMBAD database, about  $\sim 50\%$  of them are confirmed AGNs and galaxies with spectroscopically measured redshifts, and only  $\sim 1.4\%$  are confirmed Galactic objects. Spectroscopic observations of 19 unidentified objects on the RTT-150 telescope demonstrated, that 18 of them are AGNs at redshifts  $\sim 0.01-0.3$ , and one object is a M star in our Galaxy. We discuss various scenarios explaining the nature of such peculiar objects.

**Keywords:** X-ray sources, active galaxy nuclei, optical observations, proper motions

### INTRODUCTION

After more than two years of scanning the X-ray sky eROSITA telescope (Predehl et al., 2021) of the SRG Orbital X-ray Observatory (Sunyaev et al., 2021) has detected an unprecedented number of X-ray sources and localized them with high positional accuracy. One of the directions of research with the obtained catalog of X-ray sources is to search for and study stars in our Galaxy that are active in the X-ray. The GAIA catalog (Gaia Collaboration et al., 2016, 2021) is used for this purpose, which contains information on the parallaxes and proper motions of about an one and half billion optical sources on the sky. The combination of these two catalogs makes it possible to form a catalog of X-ray active stars for further study. Examining the resulting catalog, we found a small number of objects with contradictory X-ray and optical characteristics that simultaneously pointed towards both extragalactic and Galactic nature of these sources.

Similar results were independently obtained earlier by Souchay et al. (2022) – by comparing the large astrometric catalog of quasars (LQAC-5) and GAIA sources (eDR3) they identified several dozen of ex-

tragalactic sources for which GAIA measured statistically significant parallaxes and/or proper motions. An example is the brightest (in the optical band) radio quasar 3C273, which has a measurable proper motion (Gaia Collaboration et al., 2022b). On the one hand, the measurement of proper motion for spectroscopically confirmed quasars may point to errors in one of the compared catalogs. On the other hand, a possible explanation of such contradictory facts may be the displacement of the photo-center of the galaxy or its active nucleus on the scale of GAIA observations, i.e. several years with significant positional measurements. This can occur, for example, due to the motion of jets in the core or microlensing phenomena. Thus, based on new high-precision observations made for 4 extragalactic radio sources (3C 48, CTA 21, 1144+352, 1328+254) at VLBI in 2018-2021, a significant offsets of their positions from 20 to 130 milli arcsec at a time interval of over 2 decades (Titov et al., 2022) were found. The separation of such extragalactic sources from a sample of quasars and AGNs is extremely important for the task of building the fundamental GAIA coordinate system.

The present paper is dedicated to the study of such peculiar objects. In the section "Selection of sources"

\* e-mail: irek\_khamitov@hotmail.com

the methodology of selection of optical candidates of extragalactic sources with proper motions from the eROSITA catalog of X-ray stars is described. In the section "Optical identification of the sample of extended sources" we perform identification of the obtained sample by using SIMBAD database. In the section "Optical spectroscopy of candidates" the results of spectral observations of 19 earlier non-identified sources carried out on the 1.5 m Russian-Turkish RTT-150 telescope during September – October 2022 are presented. In the section "Analysis and discussion" possible scenarios that could explain the apparent proper motion of extragalactic sources are considered.

## SELECTION OF SOURCES

### *eROSITA telescope data*

In this work we used the SRG/eROSITA X-ray source catalog in the Eastern Galactic hemisphere, the processing of data on which the Russian consortium of the eROSITA telescope is responsible for. The catalogue was obtained by the X-ray catalog science working group of the Russian consortium of the eROSITA telescope. A detailed description of the procedure for the detection and characterization of sources, astrometric correction, and validation of the catalog will be given in a dedicated paper. Here we present only the basic facts. The catalog was built using the data obtained by the SRG/eROSITA telescope between December 2019 and February 2022. During this period eROSITA completed four all-sky surveys and performed a partially fifth survey covering  $\approx 38\%$  of the sky. Calibration of eROSITA telescope data, production of sky maps, detection of sources and their characterization were carried out using several components of the eSASS software developed by the German SRG/eROSITA consortium (Brunner et al., 2022) and the software developed at IKI RAS by the Russian SRG/eROSITA consortium. The data were processed using the results of ground-based calibrations and calibration observations, performed in October–November 2019. For further analysis the X-ray catalog in the energy range of 0.3–2.3 keV will be used, filtered with the detection confidence threshold corresponding to  $\approx 4\sigma$  (likelihood threshold of 10).

### *X-ray stars selection*

Galactic source candidates were selected based on a comparison with the GAIA satellite catalog. To this end, the X-ray catalog was correlated with the GAIA eDR3 catalog and the eROSITA sources were selected so, that (i) in the 98% error circle<sup>1</sup> only one source from the GAIA catalog has been found, and (ii) for

<sup>1</sup>Typical values of the 98% position error circle radius for eROSITA sources are  $\approx 5$ –20 arcsec.

this source, the GAIA satellite measured the parallax or proper motion with a signal-to-noise ratio  $S/N > 5$ . In determining the  $S/N$  of the proper motion measurement we checked both the two components of proper motion in the equatorial coordinates, as well as the total proper motion of the source. During the correlation of the eROSITA and GAIA catalogues, the positions of optical sources were corrected for their proper motion in the cases when the signal-to-noise ratio of the proper motion measurement exceeded  $S/N > 3$ .

As a result of this selection, a catalog of likely Galactic X-ray sources was obtained, which included about  $\sim 1.7 \times 10^5$  sources. The vast majority of these objects are the stars active in the X-ray range. The active binary stars, cataclysmic variables, X-ray binaries and other less numerous classes of objects are contributing as well.

We do not consider issues of completeness and purity of the resulting catalogue, as they are not crucial for the purposes of this study. These issues will be discussed in subsequent publications. The main goal of this work is the study of a small group of peculiar objects in the eROSITA catalog. At the same time we do not aim to make an exhaustive list of such objects, and their search procedure excludes chance coincidences, at least from the point of view of their optical characteristics.

Nevertheless, let us make a few general remarks. First, we should note that the above analysis was performed using 98% radius of localization of X-ray sources (localization errors of optical sources are many times smaller and are not important in this analysis). By the definition of 98% error, 2% of the objects must be outside this radius. It makes a relevant, but not decisive contribution to the completeness and purity of the resulting sample. A more important source of catalog impurity is random matches. As far as completeness with respect to Galactic objects, it is mainly determined by the fact that the X-ray sources with more than one GAIA object in the error circle were excluded.

For short, we will hereafter call the resulting sample of objects as "catalog of X-ray stars", knowing that it also includes other types of Galactic sources and has limited completeness and purity.

### *Search for extended optical sources in the catalog of X-ray stars*

In the GAIA eDR3 catalog, in addition to the integral flux in the broad photometric G-band, the fluxes in the BP and RP bands, which are (almost) two "halves" of the G band. Based on these, the parameter of color excess BP+RP (phot\_BP\_RP.excess\_factor in GAIA catalog notation), calculated as the ratio of the sum of the fluxes in the BP and RP bands to the flux in

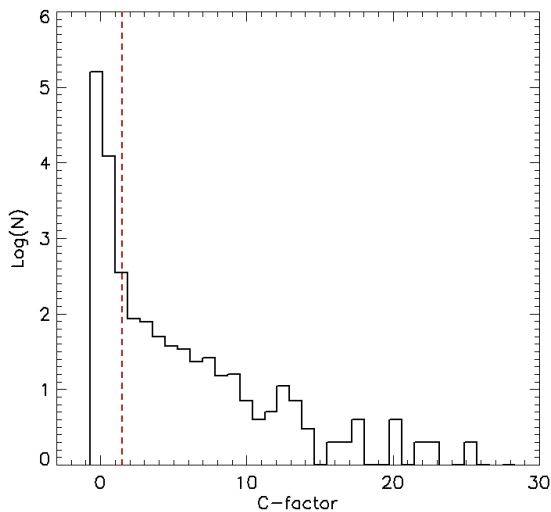


**Fig. 1.** The distribution of modified  $C^*$ -factor values for the sources of the X-ray star catalog. For the selection of candidates for optically extended objects, values above 1.5 were used, i.e., objects to the right of the vertical dashed line in this graph.

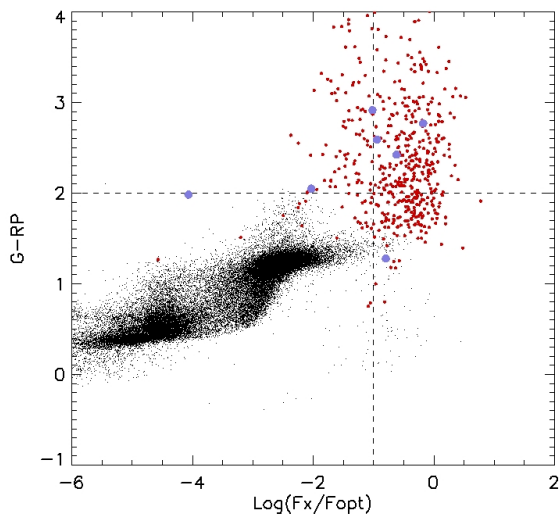


**Fig. 2.** Dependence of the  $G-RP$  color on the logarithm of the ratio of the X-ray flux measured from eROSITA data in the range 0.3–2.3 keV to the optical one, according to Gaia satellite measurements in the G-band, presented separately for a sample of close stars (black symbols) and a sample of extended objects (red symbols). Blue symbols indicate those of the candidates for optically extended objects that have been identified with Milky Way sources. The dashed lines show the conditional boundaries separating stars from galaxies, AGNs, and quasars by color and with respect to  $F_X/F_{opt}$ , see text.

the G band. In the literature, this value is sometimes denoted as  $C$  and is used to characterize the quality of GAIA satellite photometry and, in particular, as an indication of object extension (Riello et al., 2021). Despite the fact that the transmission in G-band almost completely covers the sum of BP and RP bands, due to the fact that the G-band uses narrower windows on the GAIA CCDs when transmitting data to the Earth, for extended or blended sources this  $C$  parameter will be greater than unity. For point sources, it is close to or slightly greater than unity, with some dependence on the shape of the object spectrum. In particular, because of the lower sensitivity of the G band in the red region of the spectrum as compared to the RP band, sources with emission detail can show significant value of the color excess parameter. Thus a corrected color excess factor  $C^*$  was proposed, taking into account this effect (Riello et al., 2021), which we will use further. The parameter  $C^*$  is defined so that for point sources it is close to zero (as opposed to  $C$ ). On Fig. 1 the distribution of  $C^*$ -factor values for the X-ray star catalog sources is shown.

Based on the catalog of X-ray stars, we have compiled two samples of objects. The first is all sources within 200 pc of the Sun, i.e., having a parallax  $> 5$  milli arcsec. Hereafter, we will call it the “close star sample”. It characterizes the properties of X-ray stars with a sufficient degree of completeness. The second sample is composed of sources with a corrected  $C^*$ -factor greater than 1.5, i.e., it is a sample of probably optically extended or blended objects (hereafter, the “extended object sample”). It includes 502 objects belonging to the catalog of X-ray stars. On Fig. 2 these two samples are plotted on the plane of the logarithm of the ratio of X-ray flux to optical  $F_X/F_{opt}$  and the color  $G-RP$ . The ratio  $F_X/F_{opt}$  was calculated using the X-ray flux in the 0.3–2.3 keV range and the optical flux in the G-band. The black dots show a sample of nearby stars, and the red dots show, respectively, the sources of the sample of extended objects. The horizontal dashed line shows the  $G-RP$  color boundary equal to 2, above which the galaxies are mostly located (Gaia Collaboration et al., 2022a). The vertical dashed line  $\log(F_X/F_{opt}) = -1$  is the conditional boundary between the AGN and the stars (Belvedersky et al., 2023). It is seen that in this diagram the optically extended sources are mainly located in the region typical to the active galaxies and quasars.

Thus, 502 X-ray sources were selected from the eROSITA catalog of X-ray stars, which are identified with GAIA peculiar objects. The peculiarity of the GAIA objects consists in the fact that, on the one side, they have statistically significant parallax or proper motion, which identifies them as objects in our Galaxy, and on the other side, according to GAIA’s

color excess parameter, they are probably optically extended objects. At the same time, these objects has an abnormally large measured G–RP color and/or high  $F_X/F_{\text{opt}}$  ratio, not characteristic for the stars (Fig. 2). Subsequent sections of the paper are dedicated to the study of these unusual objects.

### OPTICAL IDENTIFICATION OF A SAMPLE OF EXTENDED SOURCES

Identification of a sample of extended sources was performed using the SIMBAD database<sup>2</sup>. The search for matches was performed within a radius of 0.5 arcsec. We also found 11 matches with an accuracy of a few angular seconds, which we decided to keep in the list of matches for further study.

The results of the identification are listed in the Table 1. Totally 251 matches were found for the sources of a sample of extended objects as an extragalactic SIMBAD objects with spectroscopically measured redshifts. For 41 of them the proper motion modulus exceed 5 milli arcsec/year, and for four objects – more than 10 milli arcsec/year. Ten identified extragalactic objects with the largest proper motions are shown in the Table 2.

It should be noted that according to the results of the identification with SIMBAD we found among the sample of extended sources 6 objects of Galactic nature. Among them, 4 sources are low-mass X-ray binaries with  $C^*$ -factor ranges from 4.5 to 8.5, one M-class star and one cataclysmic variable with  $C^*$  is less than 2 (1.95 and 1.61, respectively). Moreover, the logarithm of  $F_X/F_{\text{opt}}$  exceeds  $-1$  for CV, and for the M-star is about  $-4$ . The X-ray binaries are located near the M31 galaxy and the complicated background seems to be the reason for the large values of  $C^*$ .

For the sample of sources of extended objects absent in SIMBAD a visual inspection of their morphology was performed using optical images of Pan-STARRS DR1 (Chambers et al., 2016); for this purpose web-interface of deep images PanSTARRS-1 Image Access<sup>3</sup> was used. The results of this process are shown in the bottom two rows of the Table 1. The examples of the identification of extended sources are shown on Fig. 3. Thus, a list of sources with an extended structure was compiled for further investigation of their nature by spectral observations.

### OPTICAL SPECTROSCOPY OF CANDIDATES

Optical spectroscopy was performed for 19 objects from the categories of "galaxies with unknown z" and "unknown extended sources" with G values brighter

**Table 1.** Results of identification analysis using the SIMBAD database for the sources in the sample of extended objects.

Source type	<i>N</i>
Active galaxy nuclei	182
The galaxies with measured z	69
Galaxies with unmeasured z	39
Galactic sources	6
Unknown extended	122
Unknown blended	84

than  $20^m$  and declinations above  $\geq 20$  degrees. Priority was given to objects with declinations of  $\geq 37$  degrees, since this program had the status of a pilot and observations were made during bright Moon times outside the main observational programs of optical support of the SRG observatory.

Spectral observations of these objects were carried out on the 1.5m Russian-Turkish RTT-150 telescope using the TFOSC<sup>4</sup> instrument. A CCD camera Andor iKon-L 936<sup>5</sup> was used with a  $2048 \times 2048$  pixels BEX2-DD-9ZQ light detector and a resolution element of  $0.''326$ , cooled down to  $-80^\circ$ . The quantum efficiency of the CCD detector is of 90% or higher in the wavelength range from  $4000 \text{ \AA}$  to  $8500 \text{ \AA}$ . Grism 15 was used as a disperser together with slit width of  $0.134 \text{ mm}$  ( $2.4 \text{ arcsec}$ ). During September and October 2022 low-resolution spectra were obtained in the wavelength range from  $3800 \text{ \AA}$  to  $8800 \text{ \AA}$  for 19 above mentioned candidates with a spectral resolution of  $15 \text{ \AA}$ . The spectral data were processed in a standard way using the IRAF<sup>6</sup> software, as well as with our own software using standard set of calibrations. The spectrophotometric calibration of the instrumental spectra was obtained using observations of spectrophotometric standards at the same zenith distance, as the investigated objects (Oke, 1990).

The results of spectral observations on RTT-150 are shown in Table 3. In Fig. 4 the example of identification spectrum of SRGeJ001124.6+380935 object is shown. This candidate was identified as an active galaxy nucleus of Sy2 type. Only one source of  $19 - \text{SRGeJ041510.2+824005}$  – was identified as an M-class star with a strong H $\alpha$  emission line. The remaining 18 candidates were confirmed as extragalactic sources. All of them turned out to be AGNs of various types with redshifts varying from 0.0155 to 0.272. The uncertainty of the redshift measurements is  $\delta z/(1+z) \sim 0.001$ . The redshift measurement of the source SRGeJ024443.5+204136, with a rather general determination of its type as an extragalactic object,

<sup>4</sup><https://tug.tubitak.gov.tr/en/teleskoplar/rtt150-telescope-0>

<sup>5</sup><https://andor.oxinst.com/products/ikon-xl-and-ikon-large-ccd-series/ikon-l-936>

<sup>6</sup><http://iraf.noao.edu/>

<sup>2</sup><https://simbad.cds.unistra.fr/simbad/sim-fcoo>

<sup>3</sup><https://ps1images.stsci.edu/cgi-bin/ps1cutouts>

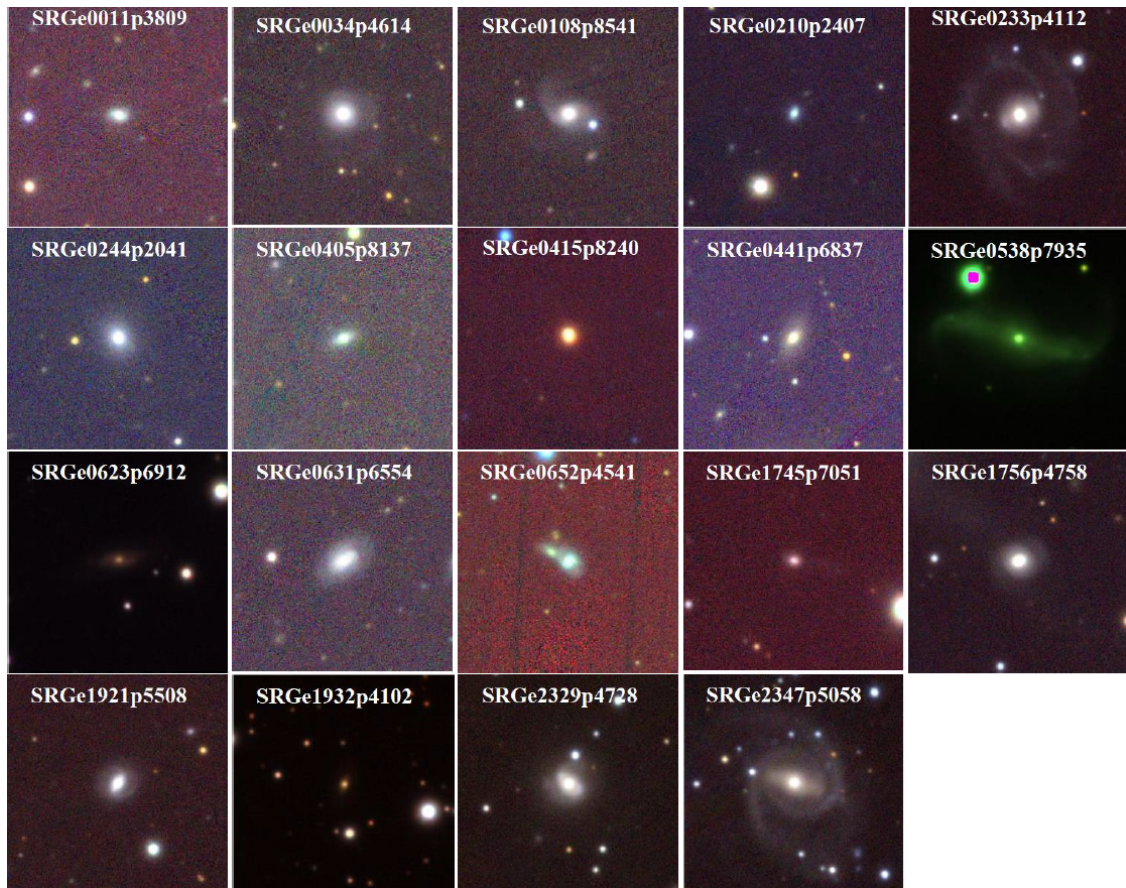


**Fig. 3.** Visual inspection of the morphology of sources, carried out using deep images of the Pan-STARRS survey. The fields of 19 sources for which spectra were obtained on RTT-150 are presented. The size of each field is  $60 \times 60$  arc sec. Only one source SRGeJ041510.2+824005 (figure identifier SRGeJ0415p8240) turned out to be an M-class star with a strong  $H\alpha$  emission line. The other candidates were confirmed as extragalactic X-ray sources with redshifts from 0.016 to 0.272, active nuclei of galaxies of various types.



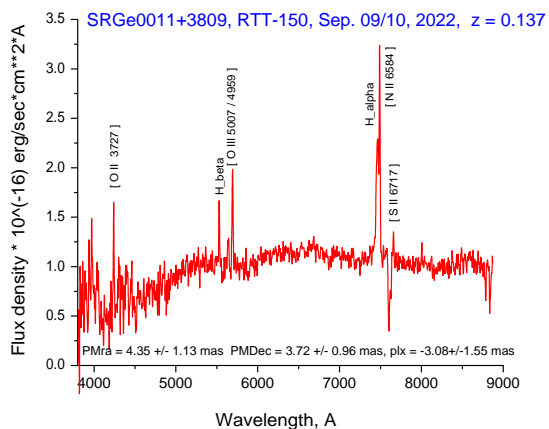


**Fig. 4.** The spectrum of SRGeJ001124.6+380935 of one of the 19 sources studied on RTT-150. The spectrum corresponds to the AGN type Sy2 at the redshift  $z = 0.137$ .

is also available in the LAMOST DR7 catalog (Wang et al., 2022),  $z = 0.050928 \pm 0.00004$ , which agrees within the accuracy of the RTT-150 data.

The program of spectral observations of the sample of extended objects which are accessible to observations on RTT-150 ( $\text{DEC} > -30^\circ$ ,  $G < 20^m$ ) will be continued. Objects fainter than  $G > 20^m$  are planned for spectral observations with telescopes of larger apertures.

## ANALYSIS AND DISCUSSION

### *Possible astrophysical explanations for the apparent proper motions of extragalactic objects*

The presence of apparent proper motions of extragalactic sources may be a result of object photocenter’s position changes, which can take place for a number of reasons of astrophysical nature. The position of the photocenter of a galaxy with an active nucleus, measured by GAIA, is determined by the sum of the contributions of the radiation from the stellar component, accretion disk, nucleus, jets, and radiation from the medium interacting with the jets. The phenomenon of the microlensing can also play a role. The variability of the different components which has a relative contributions to the registered brightness can leads to a time dependence of the optical coordinates of the AGN. The proper motion represents the average value of the photocenter position change over a period of more than 2.8 years, used in GAIA eDR3 data in the construction of astrometric solutions (Gaia Collaboration et al., 2021). Consequently, the total displacement of the photocenters ( $l$ ) of the studied objects is the value of the proper motion multiplied by the factor

$\sim 3$ . Thus, to provide the observable apparent proper motion of AGN, a few components of radiation must be at the angular distances from several units to several tens of milli arcsec, and their brightness has to vary on a scale of  $\sim 3$  years. Such angular distances correspond to linear sizes ranging from a few parsecs to several hundred parsecs, depending on the distance to the object. These distances between the components can be achieved as a result of the motion of the jet and its interaction with the environment. Indeed, in (Petrov et al., 2019), using the previously detected offsets in the positions between the VLBI radio sources (mainly AGNs) and their optical components in GAIA (Petrov & Kovalev, 2017), it was obtained that the lines of significant offsets are parallel to the direction of the jets in 62% of cases. It is also noted that the parallelism of the proper motions vector to the direction of jets takes place much more often in the case of large values of the proper motions modulus.

For an object located at a redshift of  $\sim 0.05\text{--}0.25$ , one millisecond of arc corresponds to linear size of  $\sim 1\text{--}4$  pc and, therefore, the velocities of the visible component displacements must be superluminal,  $\sim 1\text{--}10c$  in order to explain the observed proper motions. In the case of relativistic jets at velocities close to the speed of light, significant visible jet displacements are observed on the scale of a few years. For example, the Hubble Space Telescope measured the superluminal motion in relativistic jets in M87 nucleus on the order of 100 millisecond of arc per 5 years (Biretta et al., 1999). In relativistic cases the displacement of the photocenter will be determined already by the character of motion of the jet itself.

The position of the photocenter can also be influenced by the cases when a star of our Galaxy is projected onto the AGN nucleus. In this case, the parallax displacement of the photocenter should also be observed, and if the star is at the periphery of the of the Milky Way, the star’s contribution will be only in the apparent proper motion. For such cases, in the spectra of AGN the spectrum of the star itself will also be present, which can be distinguished by spectral observations with a high signal-to-noise ratio. In addition, in order to isolate such cases one of the parameters of the GAIA eDR3 catalog – the frequency of detection of multiple peaks when determining the image parameters (`ipd_frac_multi_peak`), can be used. This modulus is expressed as a percentage of detection of double peak in one-dimensional observation window to the total number of measurements (Gaia Collaboration et al., 2021). The values of this parameter in our sample do not exceeds 10%, except for the source SRGeJ184426.6+624831 with the highest proper motion value, which has a double image structure in more than half of the cases

**Table 2.** Identified extragalactic sources with spectroscopic redshift measurements that demonstrate the presence of significant apparent proper motions. The Table shows the 10 sources with the largest proper motions, in order of decreasing this value.

eROSITA (SRGe+)	GAIA eDR3	RA	DEC	sep (arcsec)	Gmag	BP-RP	$\mu$ (mas/yr)	z	Type
J184426.6+624831	2157144511215355264	18 44 26.31	+62 48 29.8	0.62	18.97	1.58	$28.09 \pm 0.89$	1.880	QSO**
J173533.5+252042*	4593766796395321344	17 35 33.35	+25 20 45.4	1.42	19.38	1.31	$17.33 \pm 0.28$	0.01476	galaxy
J131118.5+463502*	1553988166345499136	13 11 18.54	+46 35 02.3	0.27	19.45	1.27	$14.94 \pm 0.84$	0.271342	QSO**
J204113.5-381140	6682056384781697536	20 41 13.45	-38 11 37.5	5.12	19.05	0.99	$10.49 \pm 0.41$	0.020204	galaxy
J160851.4+295719	1318789194505704192	16 08 51.07	+29 57 15.0	0.18	19.91	1.62	$9.98 \pm 1.51$	0.04849	Sy2
J110503.8+505951	839151745380126336	11 05 04.21	+50 59 49.9	0.18	19.86	1.36	$9.43 \pm 1.30$	0.11829	Sy1**
J144026.2+332703	1286762448016026112	14 40 25.84	+33 27 02.6	0.24	20.82	1.46	$9.41 \pm 2.24$	0.27474	Sy1
J014417.5+314004	303683913296921728	01 44 17.27	+31 40 03.3	0.13	20.09	1.81	$9.32 \pm 1.93$	0.123625	QSO
J145425.5+464525*	1590336508929283200	14 54 25.48	+46 45 24.1	0.23	18.99	1.29	$8.99 \pm 0.81$	0.06914	Sy1
J135620.6+264356	1450823498570440832	13 56 20.70	+26 43 54.4	0.19	19.66	1.48	$8.86 \pm 1.54$	0.06178	Sy1

\* Sources with a ratio of the total displacement to the of the astrometric model discrepancy  $(\mu \times 2.8)/\epsilon_i$  is greater than 5 (see "Analysis and discussion").

\*\* Sources of the large astrometric catalog of quasars LQAC-5.

**Table 3.** Results of spectral observations on RTT-150 of 19 sources from the sample of extended objects.

eROSITA (SRGe+)	GAIA eDR3	RA	DEC	Gmag	BP-RP	$\mu_\alpha$ (mas/yr)	$\mu_\delta$ (mas/yr)	z	Type
J001124.6+380935	2877771750682930176	00 11 24.46	+38 09 33.7	19.92	1.14	$4.35 \pm 1.13$	$-3.72 \pm 0.96$	0.137	AGN
J003447.2+461429	389161012394980352	00 34 47.72	+46 14 29.3	18.87	1.38	$2.37 \pm 0.39$	$-1.87 \pm 0.32$	0.1344	AGN
J010812.2+854152	573881985223210368	01 08 11.86	+85 41 50.7	19.39	1.38	$0.33 \pm 0.60$	$-3.34 \pm 0.55$	0.0772	Sy2
J021049.7+240709	104209409979045376	02 10 49.38	+24 07 06.7	19.34	1.35	$-0.79 \pm 0.52$	$2.593 \pm 0.47$	0.1437	Sy1
J023309.6+411225*	338399652915819648	02 33 09.64	+41 12 22.5	19.16	1.34	$4.68 \pm 0.85$	$-7.46 \pm 0.94$	0.062	Sy1
J024443.5+204136	85364953204844416	02 44 43.31	+20 41 38.6	18.68	1.33	$-1.54 \pm 0.35$	$0.92 \pm 0.31$	0.0508	Sy2**
J040550.9+813716	569719612155006208	04 05 51.36	+81 37 17.2	19.25	1.54	$-0.87 \pm 0.31$	$-1.77 \pm 0.31$	0.118	Sy1
J041510.2+824005	569939106459907328	04 15 10.62	+82 40 11.8	16.76	3.17	$20.88 \pm 0.15$	$-36.98 \pm 0.11$		M-star
J044110.7+683728	495873426235161344	04 41 11.00	+68 37 29.3	19.78	1.72	$3.32 \pm 0.38$	$1.99 \pm 0.65$	0.1205	AGN
J053821.8+793515	553597546173225216	05 38 23.46	+79 35 12.7	17.53	1.38	$-2.21 \pm 0.40$	$3.66 \pm 0.46$	0.0155	AGN
J062329.3+691238	1106940173151909888	06 23 29.08	+69 12 32.6	19.93	1.68	$-2.46 \pm 0.57$	$-3.82 \pm 0.73$	0.0548	AGN
J063147.1+655440	1104230151864373888	06 31 47.43	+65 54 42.5	19.36	1.29	$-0.33 \pm 0.35$	$-1.94 \pm 0.39$	0.1075	AGN
J065210.0+454141	954093346623632512	06 52 10.08	+45 41 44.5	19.30	1.30	$0.36 \pm 0.82$	$-3.75 \pm 0.72$	0.1091	Sy2
J174514.8+705128	1639075140673511424	17 45 14.77	+70 51 26.8	19.42	1.29	$0.70 \pm 0.32$	$-2.17 \pm 0.41$	0.272	Sy1
J175610.9+475824	1363075598726822912	17 56 10.81	+47 58 24.8	18.67	1.38	$-2.43 \pm 0.37$	$-0.53 \pm 0.35$	0.0619	Sy2
J192156.1+550847	2140251786365419008	19 21 56.06	+55 08 47.1	18.36	1.21	$-3.01 \pm 0.23$	$-1.37 \pm 0.25$	0.092	Sy2
J193203.8+410244	2053551343150878336	19 32 04.02	+41 02 43.4	18.52	1.34	$-0.93 \pm 0.18$	$-0.12 \pm 0.19$	0.0835	Sy1
J232910.3+472800	1941757330160593536	23 29 10.44	+47 28 01.3	18.55	1.47	$-1.65 \pm 0.38$	$2.86 \pm 0.41$	0.04	Sy1
J234726.2+505850	1944173403888702592	23 47 26.32	+50 58 50.4	19.53	1.75	$-2.77 \pm 0.62$	$4.24 \pm 0.59$	0.0621	Sy1

\* Source with the ratio of the total displacement to the astrometric model discrepancy parameter  $(\mu \times 2.8)/\epsilon_i$  is greater than 5 (see "Analysis and discussion").

\*\* The spectral measurement of the redshift of the source is also available in the LAMOST DR7 catalog (Wang et al., 2022),  $z = 0.050928 \pm 0.00004$ .

(53%). Thus, the anomalous proper motion value of the quasar SRGeJ184426.6+624831 can be explained by the presence of a Milky Way star in the subsecond region of the source image. However, the absence of a significant parallax does not exclude the case of a double nucleus in the quasar as well.

#### *Noise characteristics in Gaia astrometric solutions*

To evaluate the quality of the GAIA astrometric solutions and their agreement with the data, we used one of the parameters of the GAIA eDR3 catalog, the so-called source noise excess  $\epsilon_i$  (astrometric\_excess\_noise). This value characterizes the discrepancy between the measured source positions and the 5-parameters astrometric model. Positive values mean that the discrepancies are higher than the statistically expected values. The significance of the value  $\epsilon_i$  itself is determined by the significance parameter D (astrometric\_excess\_noise\_sig). If  $D > 2$ , the values of  $\epsilon_i$  values are statistically significant. Excess noise characterizes various types of model and instrumental errors, which exceed errors of centroid determination. One would expect that sources with a complex and variable photocenter structure may have significant deviations from the standard 5-parameters astrometric model and correspondingly positive values of  $\epsilon_i$ . Fig.5 shows a plot of the ratio of the total photocenter displacement of the identified sources of the sample to the their source noise excess parameter ( $l/\epsilon_i$ ) depending on the value of  $\epsilon_i$  itself for close stars and extended sources. The dashed line in the graph corresponds to  $l/\epsilon_i$  equal to 5.

In Fig. 5 it is seen that the stars have a high value of signal-to-noise ratio: for them the measured proper motion  $\mu$  exceeds the excess astrometric noise  $\epsilon_i$  by  $\sim 1-2$  orders of magnitude. At the same time, for extended objects, the opposite picture is observed: the total displacement in the sky  $l$  for for most objects is only 2 to 3 times greater than the astrometric noise  $\epsilon_i$ . This may indicate some irregularity in the movement of the photometric center of the extended objects compared to the prediction of the astrometric model. The small number of objects in the catalog of extended sources with high values of signal-to-noise ratio, are probably real galactic sources with proper motions. Note that the M-class star identified by the RTT-150 observations has a ratio  $(\mu \times 2.8)/\epsilon_i \sim 200$ .

In Table 4 the 25 sources lying above this line are shown. Remarkably, that only 3 of the sources in Table 2 with the largest proper motions have  $l/\epsilon_i$  values above five. Among the sources listed in Table 4 as galaxy, according to the classification from SIMBAD, only SRGeJ192852.3-251642 has an optical spectrum, from the 6dFGS survey (Jones et al., 2009) obtained in 2003, corresponding to spectrum of ellip-

tical galaxy with [K, H] Ca, G, Mg, Na absorption lines at the redshift  $z = 0.10773$  and with the complete absence of emission lines typical for AGN. There are significant radio components for 11 sources, either in the public part of the LoTSS survey in the 120–168 MHz range (Shimwell et al., 2019), or in the VLASS northern sky survey in the 2–4 GHz (Gordon et al., 2021), which is 44% of the total number of 25 sources. These are mostly Seyfert Type 1 galaxies and quasars. Among the 4 sources that are in the HETDEX spring field of the LoTSS survey, with a size of 424 square degrees, only SRGeJ113925.5+451345 has no significant radio signal detected. Robust measurements of the radio component flux density ( $S_{\text{peak}} > 3$  mJy/beam) from VLASS data are detected for the quasar SRGeJ144924.5+321815. It should be noted that the brightness variations of AGNs have a stochastic behavior, and the registered proper motions due to changes in the photocenter associated with physical processes in these systems may change direction in the future, or completely disappear.

In conclusion, we note that in this work we used the ready-to-use GAIA astrometric solutions published in the EDR3 catalog. In choosing one or another scenario to explain the significant magnitudes of the apparent proper motion of AGN, it is necessary to analyze the traces of objects in the sky using the individual positions of sources measured by GAIA at different epochs. Such an analysis is planned to be presented in future publications. Spectrophotometric observations of the objects, which will be continued on RTT-150 and other telescopes, also play a critical role.

## CONCLUSION

Using Gaia measurements of proper motions and the value of the color excess factor, we have identified a small group of peculiar objects in the SRG/eROSITA catalog of X-ray stars. Their peculiarity according to Gaia data is determined by the fact that, on one hand, they have statistically significant measurements of parallax and/or proper motion, and on the other hand, the large value of color excess  $C^*$  are indicative of their non-zero angular extent. The sample includes 502 such objects. On the log ( $F_X/F_{\text{opt}}$ ) – color (G–RP) diagram, they are located outside the bulk population of stars, in a region more typical to a galaxies and AGNs. According to SIMBAD database, 251 sources are extragalactic and have redshifts measured by spectroscopic methods, 6 sources are known galactic objects, and 206 objects are not present in SIMBAD. The optical extension for 122 of the latter is confirmed visually using the Pan-STARRS data.

For 19 objects not presented in the SIMBAD database we performed low-resolution spectral observations on the 1.5-m telescope RTT-150 in Septem-



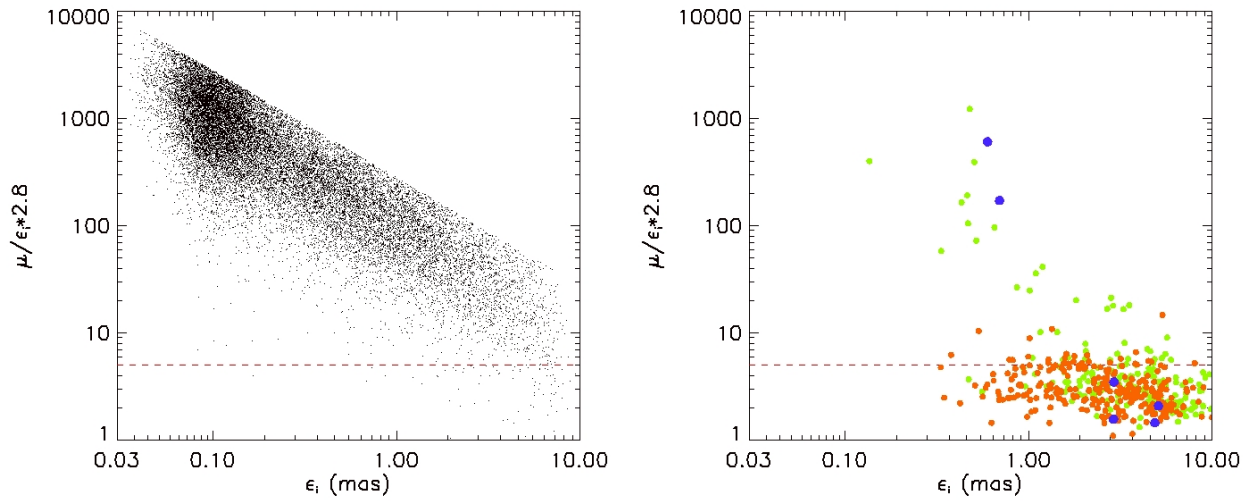


**Fig. 5.** The quality characteristics of the astrometric solutions for the catalog of nearby stars (left) and objects from the of the extended source sample (right). Both panels show only the objects for which the excess noise significance parameter  $D > 2$ . The scale is the same in both figures. The right panel shows objects whose extragalactic nature is confirmed by optical spectroscopy (orange circles), objects of our Galaxy (blue circles), and objects not identified in SIMBAD together with galaxies without spectral observations (light green circles). The dotted line shows the level of the ratio  $l/\epsilon_i = 5.0$ .

**Table 4.** Known AGN and identified on the base of spectral data obtained on RTT-150 having the ratio  $l/\epsilon_i$  greater than 5. The sources are ordered in order of decreasing proper motion.

eROSITA (SRGe+)	GAIA eDR3	RA	DEC	Gmag	$\mu$ (mas/yr)	$l/\epsilon_i$	LOFAR (mJy)	VLASS (mJy)	$z$	Type
J131118.5+463502	1553988166345499136	13 11 18.54	+46 35 02.3	19.45	14.94 ± 0.84	5.2	6.6		0.271342	QSO <sup>1</sup>
J145425.5+464525	1590336508929283200	14 54 25.48	+46 45 24.1	18.99	8.99 ± 0.81	5.4	3.7	1.71	0.06914	Sy1 <sup>2</sup>
J023309.6+411225	338399652915819648	02 33 09.64	+41 12 22.5	19.16	8.81 ± 1.24	5.4		0.63	0.062	Sy1 <sup>3</sup>
J110241.8+420655	778252648175937920	11 02 41.47	+42 06 51.9	19.35	7.02 ± 0.90	5.1			0.07498	Sy1 <sup>2</sup>
J212404.9-164149	6835161283006507520	21 24 04.81	-16 41 48.1	19.17	7.01 ± 1.09	5.0			0.03588	galaxy <sup>4</sup>
J004447.5+152910	2781106124341566976	00 44 47.34	+15 29 11.9	20.22	6.51 ± 1.17	5.7			0.2272	Sy1 <sup>2</sup>
J233515.6-085729	2438794099819112960	23 35 16.07	-08 57 23.5	20.04	5.23 ± 1.04	5.3			0.08566	galaxy <sup>2</sup>
J192852.3-251642	6766602609845906176	19 28 52.31	-25 16 38.7	19.17	5.20 ± 0.55	10.8			0.107730	galaxy <sup>4</sup>
J144227.5+555848	1607566096654997760	14 42 27.61	+55 58 46.4	18.61	4.61 ± 0.33	6.2	5.5	0.64	0.07689	galaxy <sup>2</sup>
J123740.2+611148	1580153004031345920	12 37 40.72	+61 11 48.6	19.79	4.10 ± 0.67	5.4			0.18143	Sy1 <sup>2</sup>
J002936.8-173833	2367248023501811840	00 29 36.79	-17 38 30.4	17.67	3.85 ± 0.30	6.0			0.05399	galaxy <sup>4</sup>
J021257.5+140609	77274609208701824	02 12 57.60	+14 06 10.2	18.24	3.66 ± 0.41	6.3		0.72	0.06172	Sy1 <sup>2</sup>
J143731.8+155549	1234415558406458752	14 37 31.70	+15 55 47.6	18.21	3.64 ± 0.45	5.2			0.03701	Sy1 <sup>7</sup>
J113925.5+451345	773886418783213312	11 39 25.56	+45 13 46.7	19.12	3.38 ± 0.51	5.4		0.67	0.1271	Sy1 <sup>2</sup>
J144924.5+321815	1283499819060669568	14 49 24.44	+32 18 16.2	18.37	3.29 ± 0.27	5.8		4.61	0.058	QSO <sup>6</sup>
J131447.1+260624	1447726002515875712	13 14 47.07	+26 06 24.1	18.22	3.21 ± 0.29	8.8			0.07178	Sy1 <sup>2</sup>
J195456.5-062851	4196937111313151744	19 54 56.43	-06 28 53.4	17.32	3.01 ± 0.28	5.1			0.029427	galaxy <sup>4</sup>
J010816.3-113401	2469702471186911616	01 08 16.31	-11 34 01.0	18.63	2.85 ± 0.58	5.1			0.04667	galaxy <sup>4</sup>
J070634.5+635057	1099887149653797120	07 06 34.82	+63 50 56.1	18.00	2.58 ± 0.27	5.6		0.85	0.01425	galaxy <sup>7*</sup>
J210221.6+105816	1756655887651319680	21 02 21.64	+10 58 16.0	17.78	2.39 ± 0.26	5.2		1.31	0.02893	Sy1 <sup>7</sup>
J235601.9+073123	2746340185147938304	23 56 01.95	+07 31 23.3	17.94	2.13 ± 0.35	6.0			0.040299	Sy1 <sup>8</sup>
J014458.6-023200	2505449660085848576	01 44 58.56	-02 31 59.0	17.73	1.98 ± 0.24	10.3			0.09573	galaxy <sup>4</sup>
J164313.8+095416	4446025560705238656	16 43 13.78	+09 54 16.2	17.33	1.63 ± 0.17	5.5		0.76	0.04727	galaxy <sup>7</sup>
J090436.8+553603	1035985561071454080	09 04 36.95	+55 36 02.7	17.57	1.57 ± 0.15	5.6			0.03724	Sy1 <sup>2</sup>
J224311.1+032804	2704625950939055488	22 43 11.02	+03 28 04.8	17.15	0.84 ± 0.14	6.2		2.41	0.03913	galaxy <sup>9</sup>

\* For this source, in addition to the optical component, two radio components were detected at distances of 0.5 and 0.54 arcsec from the optical component.

**Note.** The LOFAR and VLASS measurements were made in the frequency ranges 120 – 168 MHz and 2 – 4 GHz, respectively, and the values refer to the  $S_{\text{peak}}$  peak flux with a significance greater than  $5\sigma$ . Redshift measurements and source identifications were used from the following catalogs: 1 – SDSS DR7 (Abazajian et al., 2009), 2 – SDSS DR9 (Ahn et al., 2012), 3 – RTT-150 (this work), 4 – 6dFGS (Jones et al., 2009), 5 – SDSS DR11/12 (Alam et al., 2015), 6 – LAMOST (Dong et al., 2018), 7 – UZC (Falco et al., 1999), 8 – ALFALFA (Haynes et al., 2018) and 9 – 2MRS (Huchra et al., 2012).

ber - October 2022. We found 18 previously unknown AGNs with redshifts ranging from 0.0155 to 0.272. On the other hand they all have proper motions according to GAIA measurements in the range from 0.9 up to 8.8 milli arcsec/yr. One source turned out to be an M-star in the Milky Way with a strong H $\alpha$  emission line. Together with the six Galactic sources identified in SIMBAD, the fraction of confirmed Galactic sources in our sample is  $\approx 1.4\%$ .

The catalog of extended sources with proper motions will be published in a subsequent paper. The catalog can be made available to interested scientists studying such objects prior to publication upon a request to the first author of the paper.

This work is based on observations with the eROSITA telescope onboard the SRG observatory. The SRG observatory was built by Roskosmos in the interests of the Russian Academy of Sciences represented by its Space Research Institute (IKI) within the framework of the Russian Federal Space Program, with the participation of the Deutsches Zentrum fuer Luft- und Raumfahrt (DLR). The SRG/eROSITA X-ray telescope was built by a consortium of German Institutes led by MPE, and supported by DLR. The SRG spacecraft was designed, built, launched, and is operated by the Lavochkin Association and its subcontractors. The science data are downlinked via the Deep Space Network Antennae in Bear Lakes, Ussurijsk, and Baykonur, funded by Roskosmos. The eROSITA data used in this work were processed using the eSASS software system developed by the German eROSITA consortium and the proprietary data reduction and analysis software developed by the Russian eROSITA Consortium. This research has made use of the SIMBAD database, operated at CDS, Strasbourg, France. The Pan-STARRS1 Surveys (PS1) and the PS1 public science archive have been made possible through contributions by the Institute for Astronomy, the University of Hawaii, the Pan-STARRS Project Office, the Max-Planck Society and its participating institutes, the Max Planck Institute for Astronomy, Heidelberg and the Max Planck Institute for Extraterrestrial Physics, Garching, The Johns Hopkins University, Durham University, the University of Edinburgh, the Queen's University Belfast, the Harvard-Smithsonian Center for Astrophysics, the Las Cumbres Observatory Global Telescope Network Incorporated, the National Central University of Taiwan, the Space Telescope Science Institute, the National Aeronautics and Space Administration under Grant No. NNX08AR22G issued through the Planetary Science Division of the NASA Science Mission Directorate, the National Science Foundation Grant No. AST-1238877, the University of Maryland, Eotvos Lorand University

(ELTE), the Los Alamos National Laboratory, and the Gordon and Betty Moore Foundation. The work of I.M. Khamitov, I.F. Bikmaev, M.A. Gorbachev, and E.N. Irtuganov was supported by the subsidy N 671-2020-0052 of the RF Ministry of Education and Science, allocated to Kazan Federal University to fulfill the state task in the field of scientific activities. M.R. Gilfanov, P.S. Medvedev, and R.A. Sunyaev thank the support of the RNF grant 21-12-00343. The authors are grateful to TÜBİTAK, IKI, KFU, and the Academy of Sciences of the Tatarstan Republic for partial support in use of RTT-150 (Russian-Turkish 1.5-m telescope in Antalya).

## REFERENCES

1. K. N. Abazajian, J. K. Adelman-McCarthy, M. A. Agüeros, S. S. Allam, C. Allende Prieto, D. An, et al., *Astrophys. J. Suppl. Ser.*, **182**, 543 (2009)
2. C. P. Ahn, R. Alexandroff, C. Allende Prieto, S. F. Anderson, T. Anderton, B. H. Andrews, et al., *Astrophys. J. Suppl. Ser.*, **203**, id.21,13 (2012)
3. S. Alam, F. D. Albareti, C. Allende Prieto, F. Anders, S. F. Anderson, T. Anderton, et al., *Astrophys. J. Suppl. Ser.*, **219**, id.12,27 (2015)
4. M. I. Belvedersky, S. D. Bykov, and M. R. Gilfanov, *Astronomy Letters*, 49 (2023)
5. J. A. Biretta, W. B. Sparks, and F. Macchetto, *Astrophys. J.*, **520**, 621 (1999)
6. H. Brunner, T. Liu, G. Lamer, A. Georgakakis, A. Merloni, M. Brusa, et al., *Astron. Astrophys.*, **661**, A1 (2022)
7. K. C. Chambers, E. A. Magnier, N. Metcalfe, H. A. Flewelling, M. E. Huber, C. Z. Waters, et al., arXiv e-prints, p. arXiv:1612.05560 (2016)
8. X. Y. Dong, X.-B. Wu, Y. L. Ai, J. Y. Yang, Q. Yang, F. Wang, et al., *Astron. J.*, **155**, id.189,13 (2018)
9. E. E. Falco, M. J. Kurtz, M. J. Geller, J. P. Huchra, J. Peters, P. Berlind, et al., *PASP*, **111**, 438 (1999)
10. Gaia Collaboration, T. Prusti, J. H. J. de Bruijne, A. G. A. Brown, A. Vallenari, C. Babusiaux, et al., *Astron. Astrophys.*, **595**, A1 (2016)
11. Gaia Collaboration, A. G. A. Brown, A. Vallenari, T. Prusti, J. H. J. de Bruijne, C. Babusiaux, et al., *Astron. Astrophys.*, **649**, A1 (2021)
12. Gaia Collaboration, C. A. L. Bailer-Jones, D. Teyssier, L. Delchambre, C. Ducourant, D. Garabato, et al., arXiv e-prints, p. arXiv:2206.05681 (2022a)
13. Gaia Collaboration, S. A. Klioner, L. Lindegren, F. Mignard, J. Hernandez, M. Ramos-Lerate, et al., *Astron. Astrophys.*, **667**, id.A148,31 (2022b)
14. Y. A. Gordon, M. M. Boyce, C. P. O'Dea, L. Rudnick, H. Andernach, A. N. Vantyghem, et al., *Astrophys. J. Suppl. Ser.*, **255**, id.30, 17 (2021)
15. M. P. Haynes, R. Giovanelli, B. R. Kent, E. A. K. Adams, T. J. Balonek, D. W. Craig, et al., *Astrophys. J.*, **861**, id.49,19 (2018)

16. J. P. Huchra, L. M. Macri, K. L. Masters, T. H. Jarrett, P. Berlind, M. Calkins, et al., *Astrophys. J. Suppl. Ser.*, **199**, id.26,22 (2012)
17. D. H. Jones, M. A. Read, W. Saunders, M. Colless, T. Jarrett, Q. A. Parker, et al., *Mon. Not. R. Astron. Soc.*, **399**, 683 (2009)
18. J. B. Oke, *Astron. J.*, **99**, 1621 (1990)
19. L. Petrov and Y. Y. Kovalev, *Mon. Not. R. Astron. Soc.*, **467**, L71 (2017)
20. L. Petrov, Y. Y. Kovalev, and A. V. Plavin, *Mon. Not. R. Astron. Soc.*, **482**, 3023 (2019)
21. P. Predehl, R. Andritschke, V. Arefiev, V. Babyshkin, O. Batanov, W. Becker, et al., *Astron. Astrophys.*, **647**, A1, 16 (2021)
22. M. Riello, F. De Angeli, D. W. Evans, P. Montegriffo, J. M. Carrasco, G. Busso, et al., *Astron. Astrophys.*, **649**, id.A3,33 (2021)
23. T. W. Shimwell, C. Tasse, M. J. Hardcastle, A. P. Mechev, W. L. Williams, P. N. Best, et al., *Astron. Astrophys.*, **622**, A1,21 (2019)
24. J. Souchay, N. Secrest, S. Lambert, N. Zacharias, F. Taris, C. Barache, et al., *Astron. Astrophys.*, **660**, A16, 1 (2022)
25. R. Sunyaev, V. Arefiev, V. Babyshkin, A. Bogomolov, K. Borisov, M. Buntov, et al., *Astron. Astrophys.*, **656**, A132, 29 (2021)
26. O. Titov, S. Frey, Melnikov, S. Lambert, F. Shu, B. Xia, et al., *Mon. Not. R. Astron. Soc.*, **512**, 874 (2022)
27. L.-L. Wang, S.-Y. Shen, A. L. Luo, G.-J. Yang, N. Gai, Y.-K. Tang, et al., *Astrophys. J. Suppl. Ser.*, **258**, id.9,10 (2022)